Available online at www.sciencedirect.com

ScienceDirect

International Journal of Solids and Structures 44 (2007) 3497–3513

INTERNATIONAL JOURNAL OF SOLIDS and STRUCTURES

www.elsevier.com/locate/ijsolstr

The effect of a fiber loss in periodic composites

Michael Ryvkin, Jacob Aboudi *

Department of Solid Mechanics, Materials and Systems, Faculty of Engineering, Tel Aviv University, Ramat Aviv 69978, Israel

Received 23 March 2006; received in revised form 19 July 2006
Available online 11 October 2006

Abstract

Three types of analyses are combined to investigate the effect of missing fibers in periodic continuous fiber composites that are subjected to thermomechanical loadings. The representative cell method is employed in the first analysis for the construction of Green's functions elastic fields for the fiber–matrix interfacial jumps problem. As a result, the infinite domain problem is reduced, in conjunction with the discrete Fourier transform, to a finite domain problem on which Born–von Karman type boundary conditions are applied. In the second analysis, the transformed elastic field is determined by a second-order expansion of the displacement vector in terms of local coordinates, and by imposing the equilibrium equations, the interfacial traction and displacement conditions, and the Born–von Karman type boundary conditions. The actual non-periodic elastic field at any point is obtained from the Fourier-transformed fields by a numerical inversion. In the third one, a micromechanical analysis for periodic continuous fiber composites in which all fibers are perfectly bonded to the surrounding matrix provides the elastic field within the phases. A superposition of the thermoelastic fields obtained from the first and third analysis provides the traction-free boundary conditions at the interface of the missing fibers. The accuracy of the offered approach is verified by comparison with analytical solutions that exist in some special cases. Results show the effect of a missing fiber in boron/epoxy and glass/epoxy composites that are subjected to various types of thermomechanical loadings.

Keywords: Periodic composites; Representative cell method; Higher-order theory; Fiber debonding; Micromechanics

1. Introduction

Composite materials that possess periodic microstructure can be analyzed by utilizing for a given type of loading the symmetry planes of the repeating unit cell that forms the building block of the periodic composite upon which appropriate boundary conditions (that reflect these symmetries) are imposed (for transverse shear loading, however, symmetry considerations cannot be used). Another approach that can be employed in the micromechanical analysis of periodic composite is the homogenization technique which based on a two-scale expansion. The latter approach is very general since it can be employed irrespective whether plane of symmetries exist or not. The periodicity conditions (referred to as Born–von Karman boundary conditions, Ziman,

* Corresponding author. Tel.: +972 3 640 8131; fax: +972 3 640 7617.
E-mail address: aboudi@eng.tau.ac.il (J. Aboudi).

0020-7683/$ - see front matter
doi:10.1016/j.ijsolstr.2006.10.003

1964) have to be applied at the boundaries of the repeating unit cell. Reviews and of these approaches are given by Christensen (1979), Hollister and Kikuchi (1992), Nemat-Nasser and Horii (1993), Parton and Kudryavtsev (1993), and Kalamkarov and Kolpakov (1997) for example.

If, however, the periodicity of the composite is disturbed by introducing a local effect (e.g., the application of loading on just one fiber or the loss of bonding between one fiber and the surrounding matrix) the above procedures cannot be employed since a repeating unit cell on which the micromechanical analysis can be performed does not exist anymore.

The problem in which a localized thermomechanical loading is acting on a finite region of periodic composite was considered by Aboudi and Ryvkin (2006). Their analysis is based on the combination of two distinct approaches. The first one is referred to as the representative cell method (RCM) which has been presented by Nuller and Ryvkin (1980). It was further employed in the analysis of certain boundary value problems in conjunction with numerical (Ryvkin and Nuller, 1997; Moses et al., 2001) and analytical (Kucherov and Ryvkin, 2004) methods. According to the RCM, the discrete Fourier transform is applied on the periodic composite on which a local phenomena has been imposed. As a result, a representative cell problem is obtained in the transform domain upon which the Born–von Karman type boundary conditions must be implemented. Once a solution of the representative cell problem is obtained, an inverse transformation provides the thermoelastic field in any one of the cells of the composite (in particular, the neighboring cells to the localized applied loading). The second approach is referred to as higher-order theory has been employed in the analysis of functionally graded materials (Aboudi et al., 1999), the micromechanical analysis of periodic multiphase materials (Aboudi et al., 2001), the analysis of internally cooled structures (Arnold et al., 2004a) and the analysis of adhesively bonded composite joints (Bednarcyk and Yarrington, 2004; Bednarcyk et al., 2006). In the framework of this approach, the representative cell problem which has been formulated in the transform domain is discretized into several subcells. In each subcell a second-order expansion of the displacement vector is presented, and the equations of equilibrium, continuity of tractions and displacements and the Born–von Karman type boundary conditions are imposed in the average (integral) sense. The details of this analysis casted in a different and more convenient formulation are given by Aboudi and Ryvkin (2006). It should be mentioned that a reformulation of the higher-order theory has been performed by Bansal and Pindera (2003) by utilizing the continuity of displacements at the subcells interfaces. As result, the number of unknowns can be reduced by treating the average displacements at the surfaces of the subcells as the only unknowns. Furthermore, in the original higher-order theory (Aboudi et al., 1999) it was necessary to satisfy the equilibrium equations and their moments. It was shown by Bansal and Pindera (2003), however, that it is not necessary to satisfy the different moments of the equilibrium equations since in the reformulated theory they are automatically satisfied. Direct satisfaction of the equilibrium equations is sufficient. It was shown by Arnold et al. (2004b) that both the original and the reformulated theories provide identical results. In the present paper, the original formulation of the higher-order theory is employed in the form presented by Aboudi and Ryvkin (2006). It should be mentioned that this higher-order theory was originally formulated with generic cells every one of which consists of four subcells (two-level discretization) (Aboudi et al., 1999). It was shown by Aboudi and Ryvkin (2006) that by adopting a different notation in the resulting system of equations, it is more convenient to present these equations (based on the two-level discretization) in a different form that can be written (and programmed) in terms of subcells. This is in contradistinction with the reformulation of the higher-order theory that was performed by Bansal and Pindera (2003) which is genuinely based on a one-level discretization.

The problem of fibers debonding was considered by several investigators, see the recent paper by Bednarcyk et al. (2004) and references cited there. This paper addressed the effect of fiber–matrix debonding by employing, in conjunction with a micromechanical analysis, an elaborate evolving compliant interface model that was introduced by Bednarcyk and Arnold (2002). The micromechanical analysis that was employed by these authors is referred to as "high-fidelity generalized method of cells" (HFGMC) which for thermoelastic multiphase composites was developed by Aboudi et al. (2001). This micromechanical model is based on the homogenization technique and is capable to accurately predict the effective thermoelastic moduli of the composite as well as the local elastic field in the individual phases. A review of this theory and its applications in various circumstances have been presented by Aboudi (2004).

The debonding effect that was considered by Bednarcyk et al. (2004) is assumed to take place simultaneously in all fibers of the periodic composite. Consequently, the homogenization technique can be still employed since one can still identify a repeating unit cell in the damaged composite. In the present paper, a loss of one or several fibers due to a production defect or damage during service in continuous fiber composite is considered. As a result, the periodic character of the composite is lost. Here, the analysis by which this problem is approached is based on combining the RCM, the higher-order theory and the HFGMC micromechanical analysis for periodic composites. A particular ingredient in the RCM is the construction of a series of Green's functions for the non-periodic composite whose superposition with the corresponding periodic solution provided by HFGMC yields the correct traction-free boundary conditions at the interfaces of the missing fibers. The method of construction of these Green's functions was outlined by Ryvkin and Nuller (1987) and here these functions are generated for in-plane and out-of-plane (axial shear) responses. Once these Green's functions are available, the thermoelastic field of the continuous fiber composites in which several fibers are missing can be computed at any point of the non-periodic composite.

It should be emphasized that the direct use of the finite element procedure or the higher-order theory itself to analyze a composite with one or several missing fibers is very difficult and cumbersome. This is due to the fact that a repeating unit cell in the considered problem does not exist. Consequently, only the far-field boundary conditions at infinity are known. Hence, one needs to simulate a composite region occupying a large number of fibers, anticipating that the effect of the imposed inaccurate boundary conditions (which are correct only for infinite region) will diminish in the vicinity of the missing fibers, which should be located quite far away from the external boundaries. The present approach, on the other hand, allows to model an infinite region but requires the analysis of a single representative cell only which is a significant advantage.

The reliability of the method of solution is checked and verified by comparisons with the results obtained in four test cases in which analytical solutions exist. These test cases consist of an infinite plate with a hole that is subjected to: (1) uniaxial stress loading, (2) biaxial stress loading, (3) tensile and compressive in-plane loadings in two directions, and (4) axial shear loading.

Results are given for boron/epoxy and glass/epoxy composites in which one fiber is lost. The composite are subjected to axial, transverse, biaxial, in-plane shear, axial shear and thermal loadings. These results exhibit the effect on the stress field in the vicinity of the missing fiber and its rate of decay.

2. The representative cell method for periodic composites with a missing fiber

Consider an infinitely periodic unidirectional composite such that a repeating unit cell can be identified. In Fig. 1, an example of such a composite is shown in which any repeating cell is assumed to consist of a circular fiber oriented in the 1-direction, surrounded by a matrix material. It is possible, however, to consider more complicated situation such as three-phase composites with non-circular cross-section fibers. In accordance with the representative cell method (RCM) the periodic composite shown in Fig. 1 is viewed as an assemblage of bonded identical cells labeled by the two indices (K_2, K_3) where K_2, $K_3 = 0, \mp 1, \mp 2, \ldots$ The periodic composite is described with respect to global coordinates (x_1, x_2, x_3). In addition, in each cell local coordinates (x_1', x_2', x_3') are introduced whose origin is located in its center. The composite is subjected to a far-field loading $\overline{\boldsymbol{\sigma}}$. It is assumed that the fiber in the cell $(0,0)$ is missing due to damage or a production defect. Fig. 1 exhibits the case where the far-field loading is directed in the normal 3-direction. It is, however, possible to apply other types of external loadings such as a biaxial, transverse shear, axial shear or a temperature deviation ΔT, or any thermomechanical combinations. These applied loadings give rise to elastic fields in periodic composites with a missing fiber. In the present paper the resulting thermoelastic fields caused by this effect are investigated.

The thermoelastic field in the periodic composite with a missing fiber is described herein by a superposition of the following two problems:

Problem 1. The periodic thermoelastic field that is obtained in the periodic composite in which all fibers exist and are perfectly bonded to the matrix. This field can be determined from the micromechanical analysis which has been established in conjunction with the homogenization technique. This micromechanical model, referred to as "high-fidelity generalized method of cells" (HFGMC), has been fully described by Aboudi et al. (2001) where the reliability and accuracy of its predictions have been extensively discussed.

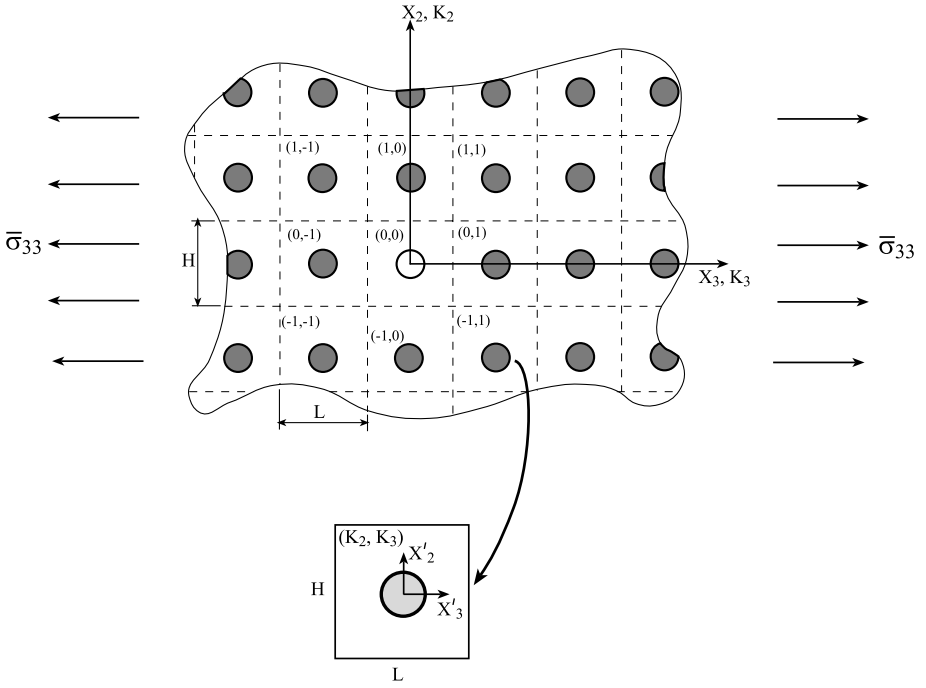

Fig. 1. A periodic composite with circular fibers oriented in the 1-direction. In every repeating cell, labeled by (K_2, K_3), local coordinates (x_2', x_3') are introduced. In cell $(0,0)$ the fiber is missing.

Problem 2. The non-periodic elastic field that is generated by a summation of auxiliary problems (Green's functions) everyone of which is a solution of a problem of a periodic composite in which all fibers exist, the far-field loading is absent and the stress field is generated by jumps in the tractions in certain parts of the fiber–matrix interface. The method of solution of this problem is based on the implementation of the higher-order theory in conjunction with the representative cell approach that has been fully described by Aboudi and Ryvkin (in press).

As will be shown in the next section, the superposition of the two solutions will generate the requested thermoelastic field of the composite with a missing fiber in such that the boundary of this particular fiber is traction-free. The missing fiber will be identified by the specific interface where these jumps in tractions have been imposed.

In the following, the solution of Problem 2 is described. In the absence of body forces, the equilibrium equations in any cell (K_2, K_3) are given by

$$[\sigma_{jk,k}]^{(K_2,K_3)} = 0 \quad j,k = 1,2,3 \tag{1}$$

where σ_{jk} are the stress components. For an elastic material they are given by

$$[\sigma_{jk}]^{(K_2,K_3)} = C_{jklm}[\epsilon_{lm}]^{(K_2,K_3)} \tag{2}$$

where C_{jklm} are the elements of the stiffness tensor of the materials occupying any cell (K_2, K_3), ϵ_{jk} are the strain tensor components. The strains are related to the displacement gradients in the standard form

$$[\epsilon_{jk}]^{(K_2,K_3)} = \frac{1}{2}\left[\frac{\partial u_j}{\partial x_k} + \frac{\partial u_k}{\partial x_j}\right]^{(K_2,K_3)} \tag{3}$$

In any cell (K_2, K_3), it is required that the displacements are continuous across the fiber–matrix interface:

$$[u_j]_{\mathrm{f}}^{(K_2,K_3)} - [u_j]_{\mathrm{m}}^{(K_2,K_3)} = 0 \tag{4}$$

As to the tractions at the fiber–matrix interface, we allow possible jumps of the tractions at certain locations there. These jumps that will be needed in the analysis may exist at the fiber–matrix interface of cell $(0,0)$ only. Thus

$$\left[\overset{(\mathbf{n})}{t_j}\right]_{\mathrm{f}}^{(K_2,K_3)} - \left[\overset{(\mathbf{n})}{t_j}\right]_{\mathrm{m}}^{(K_2,K_3)} = \overset{(\mathbf{n})}{P_j}\,\delta_{K_2,0}\delta_{K_3,0} \tag{5}$$

where $\overset{(\mathbf{n})}{t_j} = \sigma_{jk}n_k$ are the components of the traction vector, $\mathbf{n}$ is the unit normal vector at a point located on the fiber–matrix interface of cell $(0,0)$, $\delta_{p,q}$ denotes the Kronecker delta and the vector $\overset{(\mathbf{n})}{\mathbf{P}}$ represents the applied traction that accounts for the jump in the traction vector $\overset{(\mathbf{n})}{\mathbf{t}}$ at this point.

In addition, continuity of displacements and tractions between adjacent cells should be imposed. Thus,

$$\left[u_j\left(x_2' = \frac{H}{2}, x_3'\right)\right]^{(K_2,K_3)} - \left[u_j\left(x_2' = -\frac{H}{2}, x_3'\right)\right]^{(K_2+1,K_3)} = 0 \quad -\frac{L}{2} \leqslant x_3' \leqslant \frac{L}{2} \tag{6a}$$

$$\left[u_j\left(x_2', x_3' = \frac{L}{2}\right)\right]^{(K_2,K_3)} - \left[u_j\left(x_2', x_3' = -\frac{L}{2}\right)\right]^{(K_2,K_3+1)} = 0 \quad -\frac{H}{2} \leqslant x_2' \leqslant \frac{H}{2} \tag{6b}$$

and

$$\left[\sigma_{2j}\left(x_2' = \frac{H}{2}, x_3'\right)\right]^{(K_2,K_3)} - \left[\sigma_{2j}\left(x_2' = -\frac{H}{2}, x_3'\right)\right]^{(K_2+1,K_3)} = 0 \quad -\frac{L}{2} \leqslant x_3' \leqslant \frac{L}{2} \tag{7a}$$

$$\left[\sigma_{3j}\left(x_2', x_3' = \frac{L}{2}\right)\right]^{(K_2,K_3)} - \left[\sigma_{3j}\left(x_2', x_3' = -\frac{L}{2}\right)\right]^{(K_2,K_3+1)} = 0 \quad -\frac{H}{2} \leqslant x_2' \leqslant \frac{H}{2} \tag{7b}$$

Let us apply to the formulated problem (1)–(7) the double discrete Fourier transform. This provides the transformed jth component of the displacement, for example, in the form:

$$\hat{u}_j(\phi_2,\phi_3) = \sum_{K_2=-\infty}^{\infty}\sum_{K_3=-\infty}^{\infty}[u_j]^{(K_2,K_3)}\exp[\mathrm{i}(K_2\phi_2 + K_3\phi_3)] \tag{8}$$

As a result, we obtain a representative cell problem for the transforms of the field variables in the finite region $-H/2 \leqslant x_2' \leqslant H/2$, $-L/2 \leqslant x_3' \leqslant L/2$. The governing equations in this region that correspond to Eqs. (1)–(7) are:

$$\hat{\sigma}_{jk,k} = 0 \quad j,k = 1,2,3 \tag{9}$$

$$\hat{\sigma}_{jk} = C_{jklm}\hat{\epsilon}_{lm} - \Gamma_{jk}\Delta T \tag{10}$$

$$\hat{\epsilon}_{jk} = \frac{1}{2}\left[\frac{\partial\hat{u}_j}{\partial x_k} + \frac{\partial\hat{u}_k}{\partial x_j}\right] \tag{11}$$

$$[\hat{u}_j]_{\mathrm{f}} - [\hat{u}_j]_{\mathrm{m}} = 0 \tag{12}$$

$$\left[\overset{(\mathbf{n})}{\hat{t}_j}\right]_{\mathrm{f}} - \left[\overset{(\mathbf{n})}{\hat{t}_j}\right]_{\mathrm{m}} = \overset{(\mathbf{n})}{P_j} \tag{13}$$

$$\hat{u}_j\left(x_2' = \frac{H}{2}, x_3'\right) = \exp(-\mathrm{i}\phi_2)\hat{u}_j\left(x_2' = -\frac{H}{2}, x_3'\right) \quad -\frac{L}{2} \leqslant x_3' \leqslant \frac{L}{2} \tag{14a}$$

$$\hat{u}_j\left(x_2', x_3' = \frac{L}{2}\right) = \exp(-\mathrm{i}\phi_3)\hat{u}_j\left(x_2', x_3' = -\frac{L}{2}\right) \quad -\frac{H}{2} \leqslant x_2' \leqslant \frac{H}{2} \tag{14b}$$

$$\hat{\sigma}_{2j}\left(x_2' = \frac{H}{2}, x_3'\right) = \exp(-\mathrm{i}\phi_2)\hat{\sigma}_{2j}\left(x_2' = -\frac{H}{2}, x_3'\right) \quad -\frac{L}{2} \leqslant x_3' \leqslant \frac{L}{2} \tag{15a}$$

$$\hat{\sigma}_{3j}\left(x_2', x_3' = \frac{L}{2}\right) = \exp(-\mathrm{i}\phi_3)\hat{\sigma}_{3j}\left(x_2', x_3' = -\frac{L}{2}\right) \quad -\frac{H}{2} \leqslant x_2' \leqslant \frac{H}{2} \tag{15b}$$

where all field variables in the transform domain (hat-quantities) form complex quantities. Eqs. (14) and (15) refer to as the Born–von Karman type boundary conditions.

It is readily seen that one needs to solve Eqs. (9)–(15) for the representative cell where the identity of the cell (K_2, K_3) disappeared. Once this solution has been achieved by employing the higher-order theory, the actual thermoelastic field can be readily determined at any desired cell (K_2, K_3) by the inverse transform formula:

$$[u_j]^{(K_2,K_3)} = \frac{1}{4\pi^2}\int_{-\pi}^{\pi}\int_{-\pi}^{\pi}\hat{u}_j(\phi_2,\phi_3)\exp[-\mathrm{i}(K_2\phi_2+K_3\phi_3)]\,\mathrm{d}\phi_2\,\mathrm{d}\phi_3 \tag{16}$$

In practice, the solution of Eqs. (9)–(15) is determined for a spectrum of $-\pi \leqslant \phi_2 \leqslant \pi$, $-\pi \leqslant \phi_3 \leqslant \pi$ and the double integrals in (16) are approximated by the Gauss numerical integration (say), yielding

$$[u_j]^{(K_2,K_3)} \approx \frac{1}{4\pi^2}\sum_{m_2=-M_2}^{M2}\sum_{m_3=-M_3}^{M3} w_{m_2,m_3}\hat{u}_j\Big((\phi_2)_{m_2},(\phi_3)_{m_3}\Big)\exp\Big[-\mathrm{i}(K_2(\phi_2)_{m_2}+K_3(\phi_3)_{m_3})\Big] \tag{17}$$

where $(\phi_2)_{m_2}$, $(\phi_3)_{m_3}$ are the Gauss roots and w_{m_2,m_3} are the corresponding weighting factors. As it can be noted from Eq. (8), for any field variable $\hat{u}$ in the transform domain the following property holds:

$$\hat{u}(-\phi_2,-\phi_3) = \overline{\hat{u}}(\phi_2,\phi_3) \tag{18}$$

where $\overline{\hat{u}}$ denotes the complex conjugate of $\hat{u}$. Consequently, in order to obtain the value of $[u_j]^{(K_2,K_3)}$ in Eq. (17) one needs to compute $\hat{u}_j$ in the region $-\pi \leqslant \phi_2 \leqslant \pi$, $0 \leqslant \phi_3 \leqslant \pi$ only thus forming a significant saving. It can be verified from Eqs. (17) and (18) that the final value of any field variable $[u]^{(K_2,K_3)}$ is a real quantity as it is expected.

3. Construction of the Green's functions

In the framework of the micromechanical analysis of periodic continuous fiber composites that was described by Aboudi et al. (2001) the repeating unit cell is discretized into several rectangular subcells. Fig. 2 shows a discretization of the unit cell into 32×32 subcells which provides a fiber volume fraction $v_f = 0.25$.

In order to describe the construction of the Green's functions, let us consider the polygon that discretizes the circumference of the circular fiber shown in Fig. 2. It can be readily observed that the polygon possesses 16 interfacial edges in the region $0 \leqslant x_2' \leqslant H/2$, $0 \leqslant x_3' \leqslant L/2$. In Fig. 3(a), four characteristic symmetrically located interfacial edges whose unit normal $\mathbf{e}_2$ is in the x_2'-direction are shown. Four distributed out-of-plane

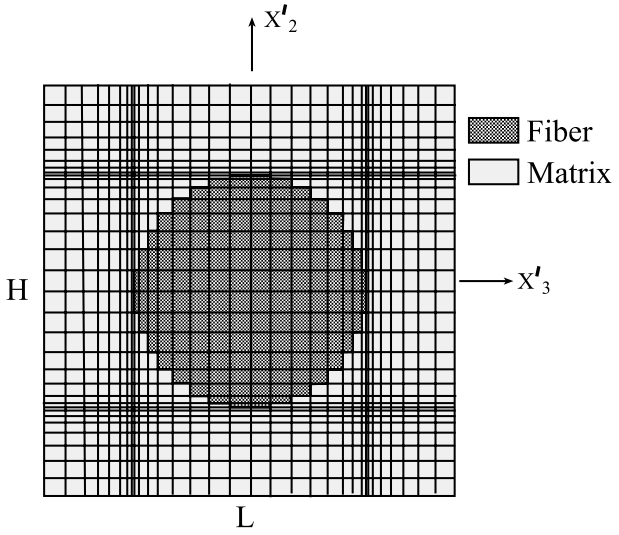

Fig. 2. The representative cell which is divided into 32×32 subcells and provides a fiber volume fraction of $v_f = 0.25$.

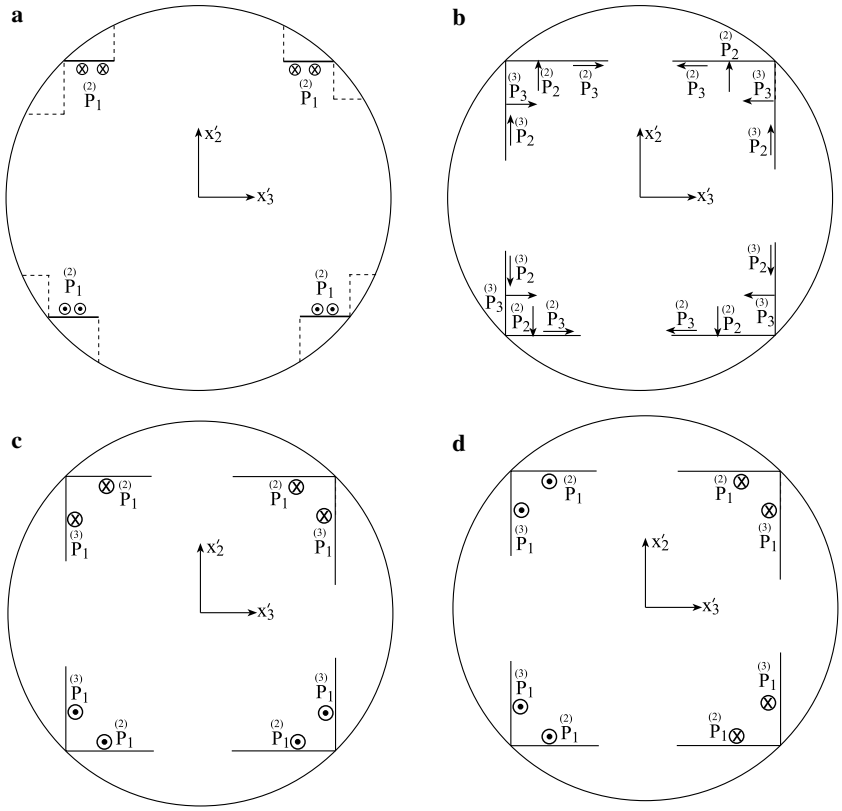

Fig. 3. (a) A characteristic fiber–matrix interface whose normal is in the 2-direction on which distributed tractions of unit magnitude are applied. (b) The in-plane (2,3) unit tractions and, (c and d) the out-of-plane unit tractions (1,2) and (1,3) that are applied on the 16 interfaces of Fig. 2 in $0 \leqslant x_2' \leqslant H/2$, $0 \leqslant x_3' \leqslant L/2$ region.

unit tractions are applied on these interfaces: $|\overset{(2)}{P_1}| = 1$ with their signs determined as shown in this figure. As a result of the application of these tractions, one can readily compute the traction resultants $\overset{(\mathbf{e}_2)}{T_j}$ and $\overset{(\mathbf{e}_3)}{T_j}$ ($j = 1,2,3$) at all 16 interfaces in matrix region. These tractions are assembled to form the vector $\overset{(\mathbf{e}_2)}{\mathbf{V}_1}$ whose length is 48. Next, we can proceed and apply this time normal tractions $|\overset{(2)}{P_2}| = 1$ at the four interfaces of Fig. 3(a). The correct signs of these normal tractions are shown in Fig. 3(b). This procedure yields the vector of interfacial traction resultants $\overset{(\mathbf{e}_2)}{T_j}$ and $\overset{(\mathbf{e}_3)}{T_j}$ which can be assembled into the 48-component vector $\overset{(\mathbf{e}_2)}{\mathbf{V}_2}$. Finally, $|\overset{(2)}{P_3}| = 1$ (see Fig. 3(b) for the appropriate signs) is applied on the same interfaces of Fig. 3(a) yielding the 48-component vector $\overset{(\mathbf{e}_2)}{\mathbf{V}_3}$. This procedure is continued for all eight such interfaces whose normal is $\mathbf{e}_2$. As a result, we obtain altogether 24 vectors $\overset{(\mathbf{e}_2)}{\mathbf{V}_p}$; $p = 1, \ldots, 24$.

The described procedure is repeated for the eight interfaces whose unit normal is $\mathbf{e}_3$ thus yielding the 24 vectors $\overset{(\mathbf{e}_3)}{\mathbf{V}_p}$; $p = 1, \ldots, 24$, the length of everyone of which is 48. In Fig. 3(b) the applied unit tractions and their appropriate directions for in-plane loading are shown, whereas in Fig. 3(c) and (d) the applied unit tractions are shown for axial shear loading in the 2- and 3-directions, respectively. Vectors $\overset{(\mathbf{e}_2)}{\mathbf{V}_p}$ and $\overset{(\mathbf{e}_3)}{\mathbf{V}_p}$, $p = 1, \ldots, 24$, are the requested Green's functions that will be employed to generate a traction-free interface that models the missing fiber.

In the framework of Problem 1, consider the 48 traction resultants on the 16 interfaces in the region $0 \leqslant x_2' \leqslant H/2$, $0 \leqslant x_3' \leqslant L/2$ of Fig. 2, that are induced due to the application of a far field on the intact composite with continuous fibers, in which all fibers exist and are perfectly bonded to the matrix. These tractions are denoted by $[\overset{(\mathbf{e}_2)}{T_j}]_b$ and $[\overset{(\mathbf{e}_3)}{T_j}]_b$, $j = 1, 2, 3$, and can be assembled into two vectors: $\overset{(\mathbf{e}_2)}{\mathbf{T}_b}$ and $\overset{(\mathbf{e}_3)}{\mathbf{T}_b}$ the length of everyone of which is 24. These tractions can be readily computed from the HFGMC micromechanical analysis that was presented by Aboudi et al. (2001).

Next, consider the following system of 48 algebraic equations

$$\mathbf{MC} = -\mathbf{T}_b \tag{19}$$

where $\mathbf{M}$ is a square matrix of the order of 48:

$$\mathbf{M} = [\overset{(\mathbf{e}_2)}{\mathbf{V}_p} \quad \overset{(\mathbf{e}_3)}{\mathbf{V}_p}], \quad p = 1, \ldots, 24$$

$\mathbf{T}_b$ is a vector of length of 48:

$$\mathbf{T}_b = \begin{Bmatrix} \overset{(\mathbf{e}_2)}{\mathbf{T}_b} \\ \overset{(\mathbf{e}_3)}{\mathbf{T}_b} \end{Bmatrix}$$

and $\mathbf{C} = [C_1, C_2, \ldots, C_{48}]$ is a vector of unknowns that can be determined by solving this system of 48 algebraic equations.

Once the vector of unknowns $\mathbf{C}$ has been determined, the elastic field $[\mathbf{U}]^{(K_2,K_3)}$ at any point Q within cell (K_2, K_3) of the continuous fiber composite in which the fiber within cell $(0,0)$ is missing can be determined as follows:

$$[\mathbf{U}]^{(K_2,K_3)}(Q) = \sum_{p=1}^{48} C_p [\mathbf{U}]_p^{(K_2,K_3)}(Q) + \mathbf{U}_b(Q) \tag{20}$$

where $[\mathbf{U}]_p^{(K_2,K_3)}(Q)$, $p = 1, \ldots, 48$, are the elastic fields at Q for the corresponding Green's functions. These fields have been determined from the inversion of the discrete Fourier transform, Eq. (17) by the application of the tractions $|\overset{(2)}{P_j}| = 1$ and $|\overset{(3)}{P_j}| = 1$ on the 16 interfaces of Fig. 2. In Eq. (20), $\mathbf{U}_b(Q)$ is the corresponding elastic field at point Q that has been obtained from the HFGMC model of the perfectly bonded intact composite. It is easily seen that the traction resultants $\overset{(\mathbf{e}_2)}{T_j}$ and $\overset{(\mathbf{e}_3)}{T_j}$ at the interfaces of the missing fiber at cell $(0,0)$ computed from Eq. (20) are indeed equal to zero for the interface in the first quadrant $x_2 \geqslant 0$, $x_3 \geqslant 0$. The interfacial tractions at the other quadrants are zero due to symmetry. The vanishing of the tractions at the fiber–matrix interface reflects the fact that this fiber is missing.

4. Applications

The present method is employed in the investigation of the effect of the loss of a fiber in the case of boron/epoxy and glass/epoxy unidirectional composites. The properties of the isotropic phases are given in Table 1. The first type of composite is characterized by a relatively high ratio between the elastic moduli of the phases while in the second one this ratio is lower. In all cases presented in this paper, 32×32 subcells has been used to discretize the representative cell, as is shown in Fig. 2. The number of Gauss's points that have been employed in the inverse transform formula, Eq. (17), is 16. These choices were checked to provide sufficient accuracy. All results in this paper are shown in the region $-2.5 \leqslant x_2/H \leqslant 2.5$, $-2.5 \leqslant x_3/L \leqslant 2.5$.

Table 1
Material constants of the constituents

	Young's modulus (GPa)	Poisson's ratio	Coefficient of thermal expansion (10^{-6} °C^{-1})
Boron	400	0.2	8
Glass	72.4	0.2	5
Epoxy	2.75	0.35	54

It is worth mentioning that the method of solution by the higher-order theory provides linear stress variations within the subcell and continuous tractions across the subcell boundaries. In addition, for the types of loading that are considered in the following, full mirror symmetry with respect to the axes passing through the center of the missing fiber exists. This was verified by checking the appropriate stress values.

4.1. Validation of the proposed approach

The reliability and accuracy of the present approach can be tested by considering an infinite thin plate with a hole. The plate is subjected to uniaxial stress loading $\overline{\sigma}_{22} = \sigma_0$ in the 2-direction (see inset of Fig. 4(b)) with all other stress components equal to zero. This is the classical Kirch's problem (cf. Timoshenko and Goodier, 1970) that generates a stress concentration factor equal to 3, and possesses a closed-form solution. In the present approach, the solution of Problem 1 in Section 2 corresponds to a plate without a hole in which the elastic field is uniform with the single non-zero component: $\sigma_{22} = \sigma_0$. Problem 2 is solved by following the approaches that were described in the previous sections, in conjunction with the higher-order theory. Fig. 4(a) and (b) presents comparisons between the predictions of the present approach and the analytical solution of Kirch's problem. It can be readily observed that both solutions coincide. At the surface of the cavity the present solution provides $\sigma_{22}/\sigma_0 = 2.7$ at $x_2 = 0$ as against the value of 3 obtained by the closed-form solution. It is obvious that by increasing the number of subcells one can further increase the former value.

It is also possible to apply a biaxial loading $\overline{\sigma}_{22} = \sigma_0$ and $\overline{\sigma}_{33} = \sigma_0$ on the thin plate with a cavity (see inset of Fig. 4(d)). In this case the analytical solution provides a stress concentration factor of 2 at the surface of the cavity. Fig. 4(c) and (d) presents a comparison between the present prediction and the analytical one. Here

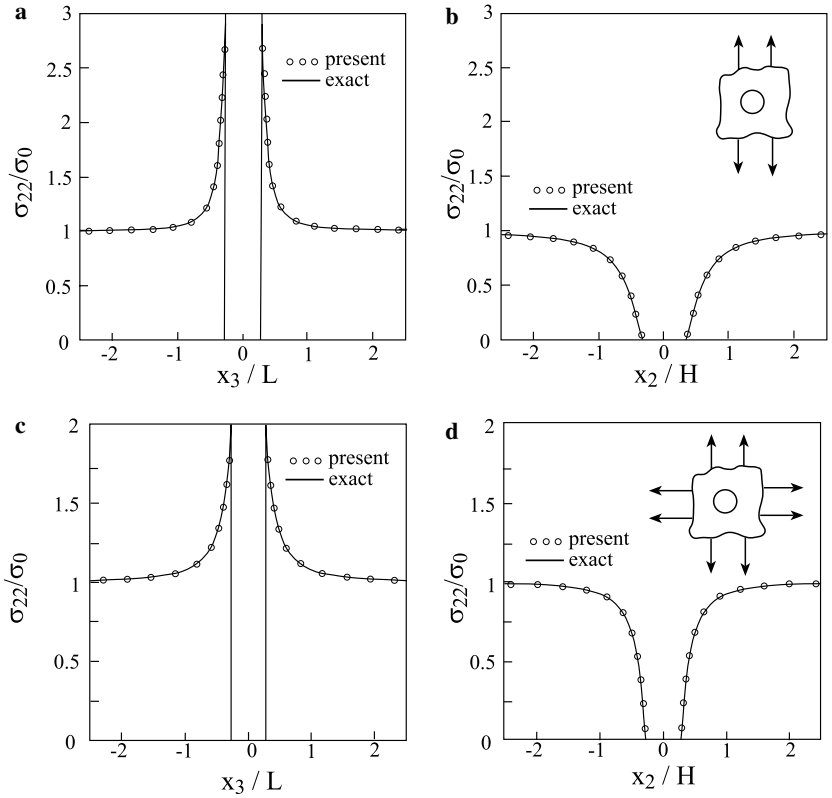

Fig. 4. (a and b) Comparison between the stresses predicted by the analytical and present solution for a thin plate with a hole subjected to a uniaxial stress loading in the x_2-direction. (c and d) Comparison between the stresses predicted by the analytical and present solution for a thin plate with a hole subjected to a biaxial stress loading in the x_2 and x_3-direction.

again up to the scale of the graph both solutions coincide. The present solution provides a concentration factor of 1.8 as against 2.

The third test case for the reliability of the present approach is obtained by subjecting the plate with a hole to a normal tensile stress loading $\overline{\sigma}_{22} = \sigma_0$ in the 2-direction and a compressive normal stress $\overline{\sigma}_{33} = -\sigma_0$ in the 3-direction, see inset of Fig. 5(b). As it is well known, the solution of Kirch's problem can be utilized to obtain closed-form expression for the elastic field that corresponds to plate with a hole subjected to in-plane shear. Fig. 5(a) and (b) exhibits a comparison between the prediction of the present approach and the corresponding analytical solution. The present solution provides a stress concentration factor of 3.5 against the value of 4 obtained by the latter.

Finally, let us consider a plate with hole that is subjected to axial shear loading: $\overline{\sigma}_{12} = \sigma_0$, see inset of Fig. 5(d). An analytical solution to this problem can be established in the form

$$\sigma_{r1} = \sigma_0\left(1 - \frac{a^2}{r^2}\right)\cos\theta, \quad \sigma_{\theta 1} = -\sigma_0\left(1 + \frac{a^2}{r^2}\right)\sin\theta \tag{21}$$

where a is the radius of the hole, r is the radial distance from its center and the angle θ is measured from the x_2 axis of Fig. 1. Comparisons of the axial shear stress σ_{12} along the axes obtained from this solution and the present approach for a plate with hole are shown in Fig. 5(c) and (d). The two solutions coincide. The stress concentration factor predicted by Eq. (21) is seen to be equal to 2, whereas the present approach provides the value of 1.9.

4.2. Mechanical loadings

Consider a the periodic composite with a missing fiber as shown in Fig. 1. The composite is loaded in the axial (fiber) direction such that $\overline{\sigma}_{11} = \sigma_0$ with all other far-field stress components equal to zero. In Fig. 6, comparisons between the axial stresses σ_{11} that are generated in the boron/epoxy and glass/epoxy composites are

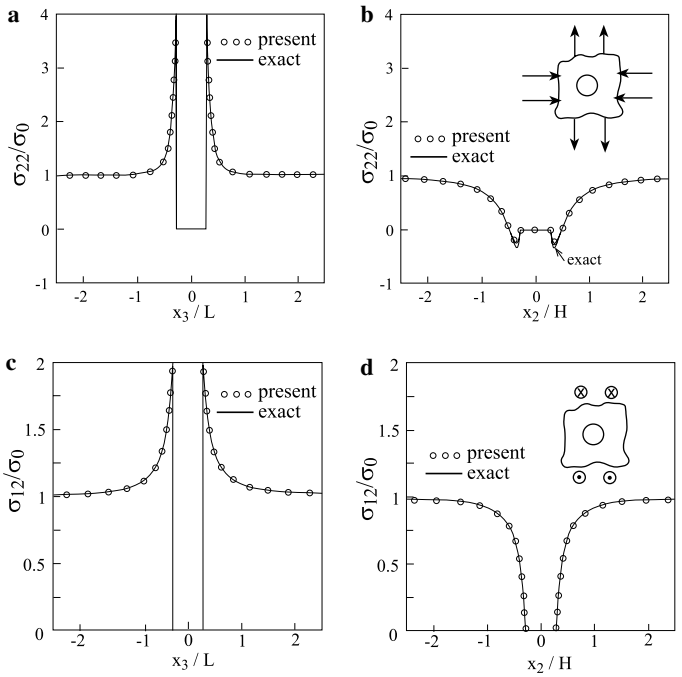

Fig. 5. (a and b) Comparison between the stresses predicted by the analytical and present solution for a thin plate with a hole subjected to tensile and compressive stresses in the x_2 and x_3-direction, respectively. (c and d) Comparison between the stresses predicted by the analytical and present solution for a plate with a hole subjected to axial shear loading.

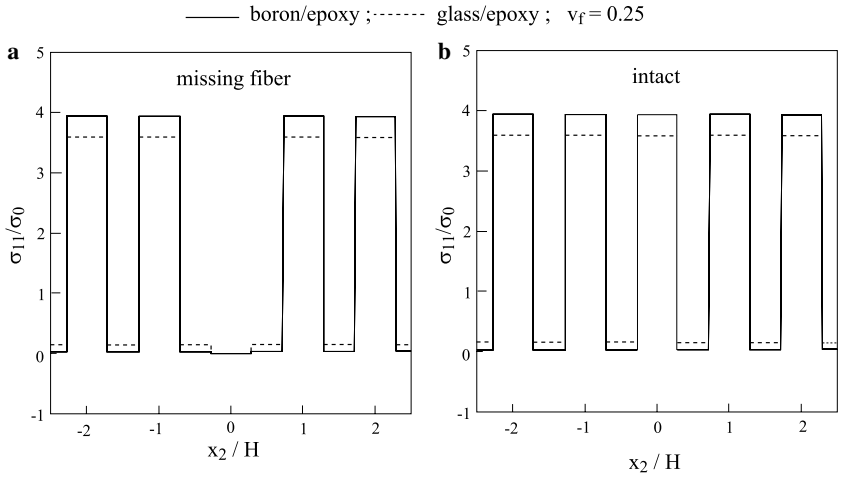

Fig. 6. Comparison between the axial stress variations σ_{11} in boron/epoxy and glass/epoxy composites ($v_f = 0.25$) due to a far-field uniaxial stress loading $\overline{\sigma}_{11} = \sigma_0$ in the fiber direction. (a) The composites are with a missing fiber, (b) intact composites.

presented. In both cases the fiber volume fraction is $v_f = 0.25$. Also shown are the corresponding stress variations in the intact composite. This figure shows that the effect of the missing fiber is localized in its vicinity. This result can be expected since for a loading in the fibers direction, their effect is dominant as they carry most of the load. This is also reflected by comparing the stress variations in the boron/epoxy and glass/epoxy composites which show a somewhat lower stress values in the glass fibers that possess lower elastic modulus.

Fig. 7 displays a comparison between the stresses σ_{22} along x_2 and x_3-axes that result from the missing fiber and intact composites. The far-field loading is given by $\overline{\sigma}_{22} = \sigma_0$ which is in a direction perpendicular to the fibers. It can be readily observed from Fig. 7(a) that $\sigma_{22} = 0$ at missing fiber interface as is expected. This figure shows that the effect of the missing fiber is significant but it decays as the distance increases. Fig. 7(b) shows that at the missing fiber interface a stress concentration is obtained that resembles the behavior in Fig. 4(a) in Kirch's problem. Fig. 7(b) shows that the effect of missing fiber decays along x_3-axis more rapidly as the distance increases. It is interesting to note that due to the releasing effect of the hole, the stresses in the fibers neighboring the missing one decrease in the loading x_2-direction, see Fig. 7(a). On the other hand, as a result of their redistribution, the stresses increase in the perpendicular x_3-direction as shown in Fig. 7(b).

The resulting stress concentration near the missing fiber can be compared with the stress concentration in Kirch's problem, Fig. 4(a) whose value is 3. A color plot of σ_{22} distribution is shown in Fig. 7(c). This plot clearly displays the concentration of stresses in the vicinity of the missing fiber and its effect on the surrounding region.

The effect of reinforcement volume fraction on response of a composite with a missing fiber can be investigated by considering a boron/epoxy composite with two values of fiber volume ratio: $v_f = 0.25$ and 0.4. Both composites are loaded in the transverse direction to the fibers ($\overline{\sigma}_{22} = \sigma_0$). A comparison between the resulting stresses σ_{22} are shown in Fig. 8. Fig. 8(a) shows the stresses against x_2 which except for the different locations of the interface of the missing fibers show quite similar behavior. The variation of σ_{22} against x_3 is exhibited in Fig. 8(b). Here, one can observe that the stress concentration at the missing fiber interface in the composite with the fiber volume fraction $v_f = 0.4$ is lower than the composite with $v_f = 0.25$. This observation can be explained by the increase of the composite's stiffness with increasing v_f, which limits the amount of strains that can develop at the vicinity of the hole.

For a biaxial loading $\overline{\sigma}_{22} = \sigma_0$ and $\overline{\sigma}_{33} = \sigma_0$ in the transverse directions to the fibers, comparisons between the transverse stress variations σ_{22} that are induced in the missing fiber composite and the corresponding intact one are shown for boron/epoxy (in both cases $v_f = 0.25$). The effect of the missing fiber can be clearly noticed in Fig. 9, where the stress concentration at the missing fiber interface can be compared with the one shown in Fig. 4(c) for a biaxially stretched plate with hole where the stress concentration is equal to 2. Here too, the increase of the stiffness of the reinforced composite as compared to the corresponding case of a hole in a homogeneous plate (Fig. 4(c)) decreases the stress concentration.

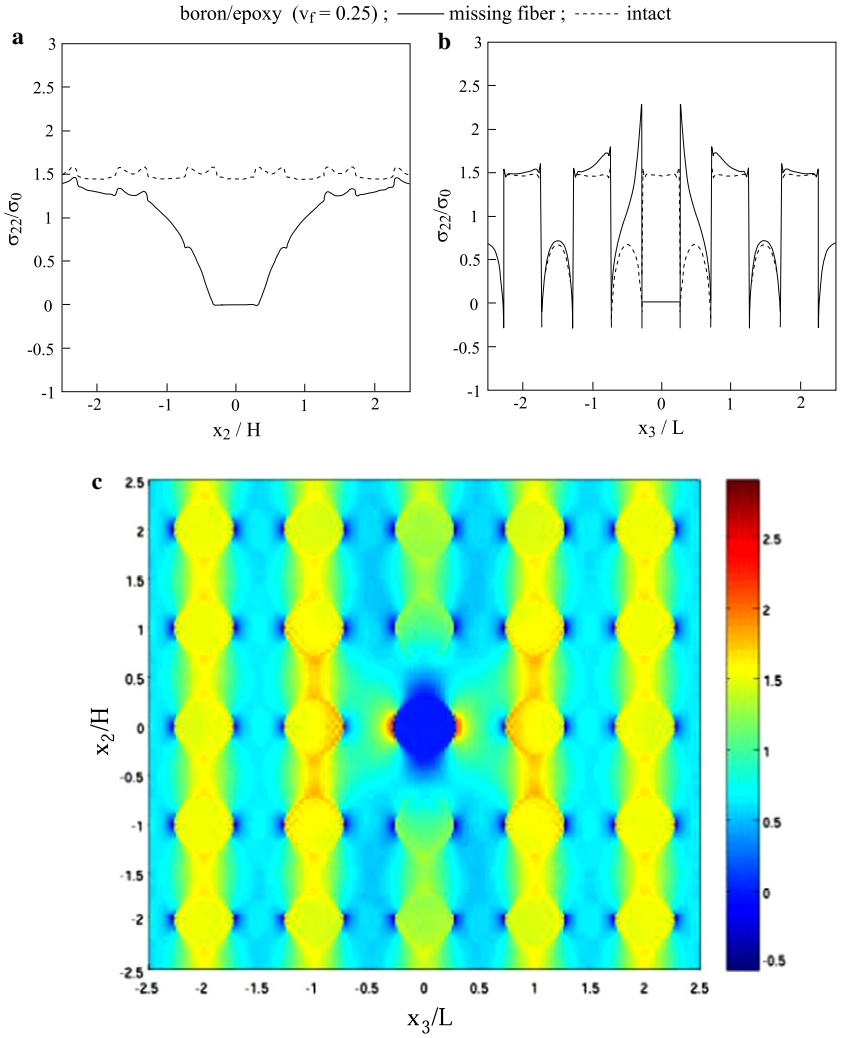

Fig. 7. Comparison between the transverse stress variations σ_{22} in boron/epoxy composite ($v_f = 0.25$) with a missing fiber and the intact one. The composites are loaded by a uniaxial far-field stress $\overline{\sigma}_{22} = \sigma_0$ in the transverse direction to the fibers. (a) Stress variation along x_2, (b) along x_3. (c) Stress σ_{22} distribution in the missing fiber composite in the region $-2.5 \leqslant x_2/H \leqslant 2.5$, $-2.5 \leqslant x_3/L \leqslant 2.5$.

Consider next the missing fiber composite that is subjected to a far-field transverse shear loading $\overline{\sigma}_{23}$. Instead, as in the case of a plate with a hole that was shown in Fig. 5(a) and (b), we subject the boron/epoxy composite ($v_f = 0.25$) to transverse tensile $\overline{\sigma}_{22} = \sigma_0$ and compressive $\overline{\sigma}_{33} = -\sigma_0$ stress loadings. The resulting transverse stress $\overline{\sigma}_{22}$ variations along the axes are shown in Fig. 10 together with the corresponding stresses obtained in the intact composite. The stress concentration Fig. 10(b) at the missing fiber interface can be compared to the case of a plate with hole that is shown in Fig. 5(a) in which the stress concentration factor is 3. A color plot of σ_{22} distribution is shown in Fig. 10(c). This plot clearly displays the concentration of stresses in the vicinity of the missing fiber and its effect on the surrounding region.

A final illustration of the effect of missing fiber in composites subjected to mechanical loadings is given in the case of a far-field axial shear loading $\overline{\sigma}_{12} = \sigma_0$. Fig. 11 shows the variations of the axial shear stresses in a boron/epoxy composite ($v_f = 0.25$) with a missing fiber and is contrasted with the corresponding case of intact composite. As in the case of in-plane loading (Fig. 7), one can observe that the axial shear stresses in the fibers neighboring the missing one decrease in the x_2-direction (namely, the direction of the remote stress gradient) and increase in the x_3-direction. A color plot of σ_{12} distribution is shown in Fig. 11(c). This plot shows that there is no stress concentrations in the vicinity of the missing fiber, but it displays its effect on the surrounding

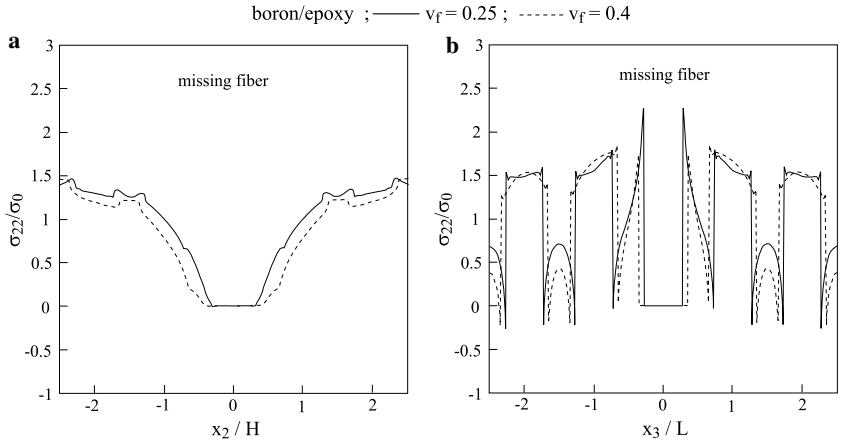

Fig. 8. Comparison between the transverse stress variations σ_{22} in boron/epoxy composite with fiber volume fraction of $v_f = 0.25$ and 0.4 both with a missing fiber. The composites are loaded by a uniaxial far-field stress $\overline{\sigma}_{22} = \sigma_0$ in the transverse direction to the fibers. (a) Stress variation along x_2, (b) along x_3.

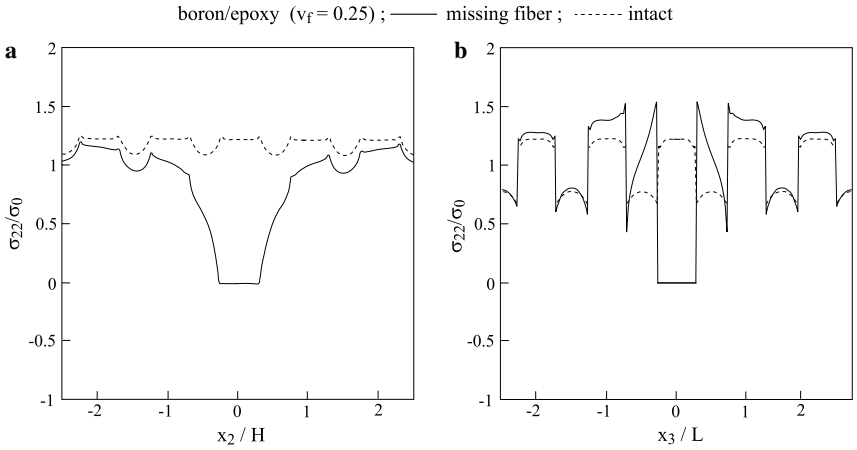

Fig. 9. Comparison between the transverse stress variations σ_{22} in boron/epoxy composite ($v_f = 0.25$) with a missing fiber and the intact one. The composites are loaded by a biaxial far-field stress $\overline{\sigma}_{22} = \sigma_0$ and $\overline{\sigma}_{33} = \sigma_0$ in the transverse directions to the fibers. (a) Stress variation along x_2, (b) along x_3.

region. It is worth mentioning that it can be shown that the elastic field generated by axial shear loadings (namely $\overline{\sigma}_{12}$ and $\overline{\sigma}_{13}$) in continuous fiber composites is not coupled to the elastic field generated by normal and transverse shear loadings. Thus, these fields can be treated independently.

4.3. Thermal loading

Thus far the composites with a missing fiber were subjected to far-field mechanical loadings. Presently, the composite is subjected to thermal loading by applying a uniform temperature deviation $\Delta T = 1$ °C from a reference temperature in the absence of mechanical loading, namely $\overline{\sigma}_{jk} = 0$. For a boron/epoxy composite ($v_f = 0.25$), the transverse stress $\overline{\sigma}_{22}$ variations along the axes are shown in Fig. 12 and contrasted with the corresponding case of intact composite. This figure displays the stress field caused by the fiber loss. The effect of the missing fiber is seen to be decaying rapidly. A color plot of σ_{22} distribution is shown in Fig. 12(c). This plot shows that there is no stress concentrations in the vicinity of the missing fiber, but it displays its effect on the surrounding region.

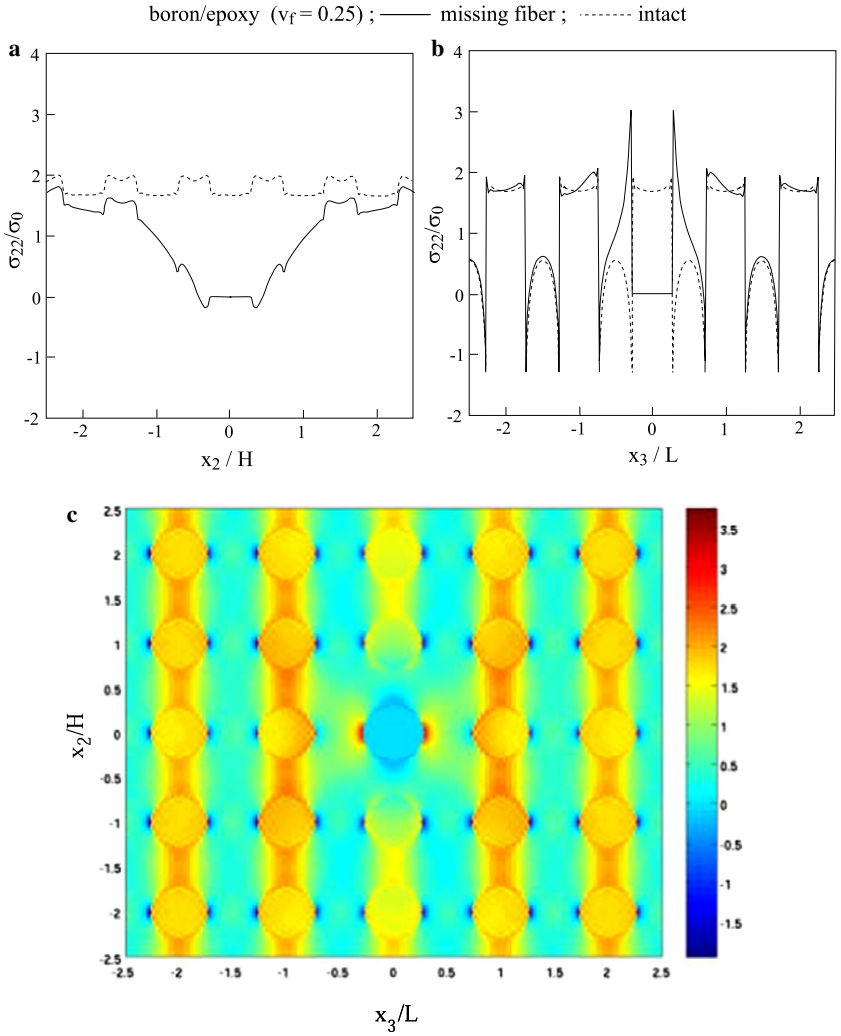

Fig. 10. Comparison between the transverse stress variations σ_{22} in boron/epoxy composite ($v_f = 0.25$) with a missing fiber and the intact one. The composites are loaded by a far-field stress $\overline{\sigma}_{22} = \sigma_0$ and $\overline{\sigma}_{33} = -\sigma_0$ which generates transverse shear loading. (a) Stress variation along x_2, (b) along x_3. (c) Transverse stress σ_{22} distribution in the missing fiber composite in the region $-2.5 \leqslant x_2/H \leqslant 2.5$, $-2.5 \leqslant x_3/L \leqslant 2.5$.

5. Conclusions

Three distinct approaches have been combined to analyze the effect of a missing fiber in periodic continuously reinforced composites that are subjected to various types of thermomechanical loadings. Stress variations in boron/epoxy and glass/epoxy composites with a missing fiber were presented along its axes of symmetry as well as surface plots of the stress distributions in its vicinity. The results show the effect of the fiber loss at its vicinity and the rate of decay of the elastic field in the composite away from the missing fiber.

In the developed theory and its application, a single fiber was assumed to be missing. It is possible, however, to consider the loss of several fibers. To this end, consider a composite in which M fibers are missing. Assume that the interfacial polygon that models a fiber–matrix interface includes N interfacial edges (for the problem that was considered in Fig. 2, $N = 16 \times 4$). Consequently, the total number of edges at the missing fiber–matrix interfaces, where traction-free conditions must be obtained, will be $N \times M$.

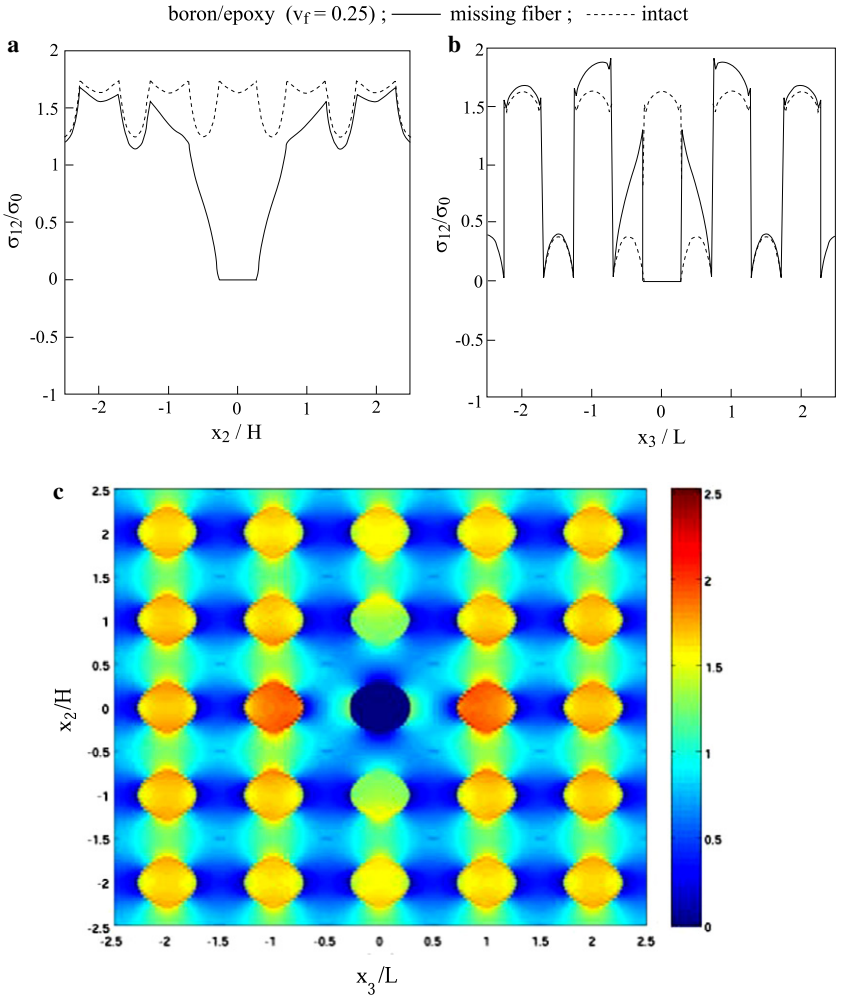

Fig. 11. Comparison between the axial shear stress variations σ_{12} in boron/epoxy composite ($v_f = 0.25$) with a missing fiber and the intact one. The composites are loaded by an axial shear far-field stress $\bar{\sigma}_{12} = \sigma_0$. (a) Stress variation along x_2, (b) along x_3. (c) Axial shear stress σ_{12} distribution in the missing fiber composite in the region $-2.5 \leqslant x_2/H \leqslant 2.5$, $-2.5 \leqslant x_3/L \leqslant 2.5$.

Since every traction vector includes three components, the order of the system (19) for establishing the Green's function coefficients **C** is $3 \times N \times M$. It should be emphasized that due to the translational symmetry of the composite's microstructure, it is sufficient to consider just $3 \times N$ types of loadings at the circumference of one fiber in order to establish the matrix **M** of the assembled traction resultants for M missing fibers. However, contrary to the case of the single fiber loss considered in the paper, the mirror symmetry of the stresses with respect to the x_2 and x_3 axes in the case of several missing fibers does not exist anymore. Hence, one cannot further reduce the number of Green functions to $3 \times N/4$ as was done in the case of one missing fiber.

It should be mentioned that solving the problem of a composite with missing fibers by a direct approach (e.g., a finite element procedure in which the composite is modeled by a sufficiently large finite region) would require, due to the strong gradients that exist in the non-periodic stress field, a tremendous amount of degrees of freedom to capture these gradients. In the present approach, on the other hand, one needs to analyze just one single representative cell.

The present approach can be extended to the case of fibers breakage or loss of bonding of inclusions in composites. To this end, one needs to combine the RCM, the higher-order theory and the HFGMC micromechanical model, all of which must be formulated in a three-dimensional form.

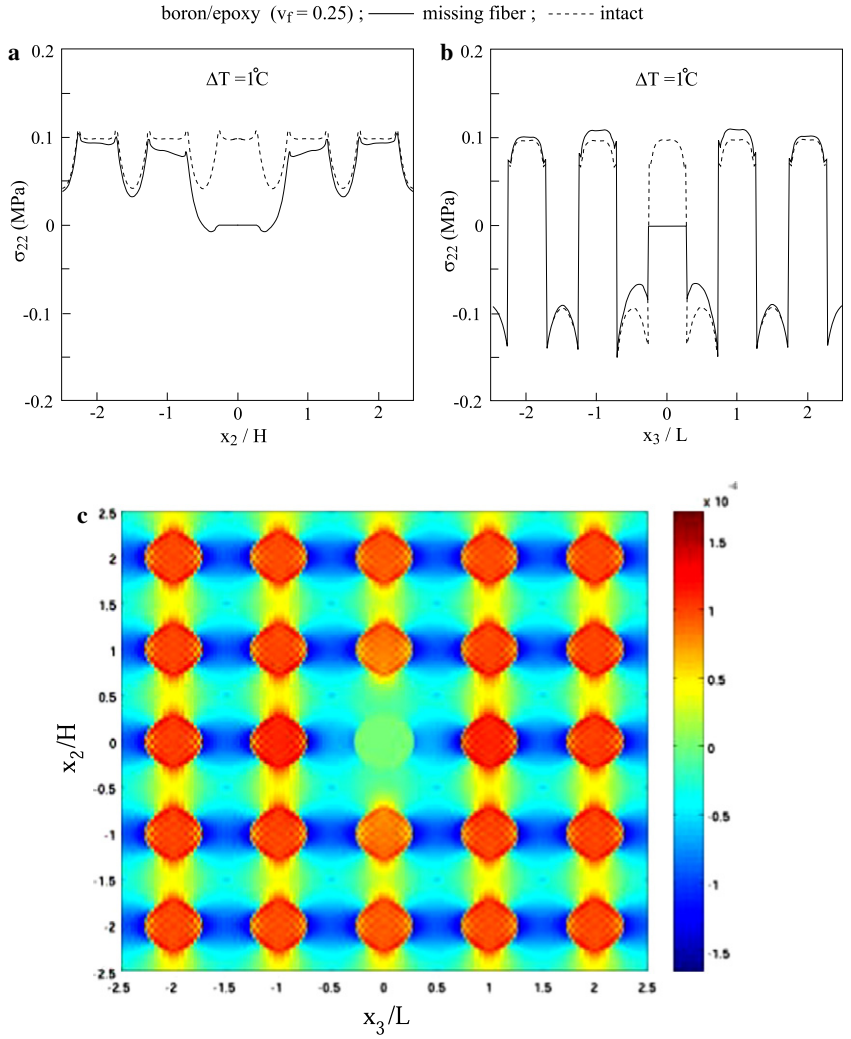

Fig. 12. Comparison between the transverse stress variations σ_{22} in boron/epoxy composite ($v_f = 0.25$) with a missing fiber and the intact one. The composites are subjected to a thermal loading in the form of a temperature deviation $\Delta T = 1$ °C from a reference temperature in the absence of far-field stresses. (a) Stress variation along x_2, (b) along x_3. (c) Transverse stress σ_{22} distribution in the missing fiber composite in the region $-2.5 \leqslant x_2/H \leqslant 2.5$, $-2.5 \leqslant x_3/L \leqslant 2.5$.

Acknowledgment

The second author gratefully acknowledges the support of the Diane and Arthur Belfer chair of Mechanics and Biomechanics.

References

Aboudi, J., 2004. The generalized method of cells and high-fidelity generalized method of cells micromechanical models – a review. Mech. Adv. Mater. Struct. 11, 329–366.

Aboudi, J., Pindera, M.-J., Arnold, S.M., 1999. Higher-order theory for functionally graded materials. Composites: Part B: Engineering 30, 777–832.

Aboudi, J., Pindera, M.-J., Arnold, S.M., 2001. Linear thermoelastic higher-order theory for periodic multiphase materials. J. Appl. Mech. 68, 697–707.

Aboudi, J., Ryvkin, M., 2006. Analysis of local effects in fiber-reinforced periodic composites. Mech. Mater., in press, doi:10.1016/j.mechmat.2006.01.003.

Arnold, S.M., Bednarcyk, B.A., Aboudi, J., 2004a. Analysis of internally cooled structures using a higher order theory. Comput. Struct. 82, 659–688.

Arnold, S.M., Bednarcyk, B.A., Aboudi, J., 2004b. Comparison of the computational efficiency of the original versus reformulated high-fidelity generalized method of cells. NASA/TM-2004-213438.

Bansal, Y., Pindera, M.-J., 2003. Efficient reformulation of the thermoelastic higher-order theory for functionally graded materials. J. Therm. Stresses 26, 1055–1092.

Bednarcyk, B.A., Arnold, S.M., 2002. Transverse tensile and creep modeling of continuously reinforced titanium composites with local debonding. Int. J. Solids Struct. 39, 1987–2017.

Bednarcyk, B.A., Arnold, S.M., Aboudi, J., Pindera, M.-J., 2004. Local field effects in titanium matrix composites subject to fiber–matrix debonding. Int. J. Plasticity 20, 1707–1737.

Bednarcyk, B.A., Yarrington, P.W., 2004. Elasto-plastic analysis of tee joints using HOT-SMAC. NASA/CR-2004-213067.

Bednarcyk, B.A., Zhang, J., Collier, C.S., Banasl, Y., Pindera, M.-J., 2006. Analysis tools for adhesively bonded composite joints, Part I: higher-order theory. AIAA J. 44, 171–180.

Christensen, R.M., 1979. Mechanics of Composite Materials. Wiley, New York.

Hollister, S.J., Kikuchi, N., 1992. A comparison of homogenization and standard mechanics analyses for periodic porous composites. Comput. Mech. 10, 73–95.

Kalamkarov, A.L., Kolpakov, A.G., 1997. Analysis, Design and Optimization of Composite Structures. Wiley, New York.

Kucherov, L., Ryvkin, M., 2004. Elastic solutions for periodically layered strip with perfect bonding or with an interface crack. Int. J. Solids Struct. 41, 4551–4565.

Moses, E., Ryvkin, M., Fuchs, M.B., 2001. A FE methodology for the static analysis of infinite periodic structures under general loading. Comput. Mech. 27, 369–377.

Nemat-Nasser, S., Horii, M., 1993. Micromechanics: Overall Properties of Heterogeneous Materials. North-Holland, New York.

Nuller, B., Ryvkin, M., 1980. On boundary value problems for elastic domains of a periodic structure deformed by arbitrary loads. In: Proceedings of the State Hydraulic Institute, vol. 136. Energia, Leningrad, pp. 49–55 (in Russian).

Parton, V.Z., Kudryavtsev, B.A., 1993. Engineering Mechanics of Composite Structures. CRC Press, Boca Raton, FL.

Ryvkin, M., Nuller, B., 1997. Solution of quasi-periodic fracture problems by the representative cell method. Comput. Mech. 20, 145–149.

Ryvkin, M., Nuller, B., 1987. Boundary-value problems for the domains contained in non-homogeneous translationally-symmetric space. In: Proceedings of the State Hydraulic Institute, vol. 202. Energia, Leningrad, pp. 11–14 (in Russian).

Timoshenko, S.P., Goodier, J.N., 1970. Theory of Elasticity. McGraw-Hill, New York.

Ziman, J.M., 1964. Principles of the Theory of Solids. Cambridge University Press, Cambridge, MA.